A new look at extensional rheology of low-density polyethylene

Huang, Qian; Mangnus, Marc; Alvarez, Nicolas J.; Koopmans, Rudy; Hassager, Ole

Published in:
Rheologica Acta

Link to article, DOI:
10.1007/s00397-016-0921-z

Publication date:
2016

Document Version
Peer reviewed version

A New Look at Extensional Rheology of Low-density Polyethylene

Qian Huang[1], Marc Mangnus[2], Nicolas J. Alvarez[3], Rudy Koopmans[2], and Ole Hassager[1]

[1] *Department of Chemical and Biochemical Engineering, Technical University of Denmark, Lyngby, Denmark*
[2] *Dow Europe GmbH, Horgen, Switzerland*
[3] *Department of Chemical and Biological Engineering, Drexel University, Philadelphia, United States*

(Dated: Feb. 10, 2015)

Abstract

The nonlinear rheology of three selected commercial low-density polyethylenes (LDPE) is measured in uniaxial extensional flow. The measurements are performed using three different devices including an extensional viscosity fixture (EVF), a home made filament stretching rheometer (DTU-FSR) and a commercial filament stretching rheometer (VADER-1000). We show that the measurements from the EVF are limited by a maximum Hencky strain of 4, while the two filament stretching rheometers are able to probe the nonlinear behavior at larger Hencky strain values where the steady state is reached. With the capability of the filament stretching rheometers, we show that LDPEs with quite different linear viscoelastic properties can have very similar steady extensional viscosity. This points to the potential for independently controlling shear and extensional rheology in certain rate ranges.

1 Introduction

Control of the rheological behavior of polymer fluids as a function of molecular chemistry has attracted a great interest in both academia and industry for many years. The most successful and prolific theory for predicting the rheological behavior of entangled polymer systems is the "tube model" proposed by Doi, Edwards, and de Gennes [1, 2]. However, despite the efforts of modifying the tube model for three decades, the nonlinear rheological behavior of entangled polymers in extensional flow is still not fully understood even for the simplest cases, i.e. monodisperse linear polymer systems [3, 4]. Industrial polymers such as low-density polyethylenes (LDPE) are among the most complex examples of entangled polymer systems. They are not only highly polydisperse, but also containing different branched molecular structures. Predicting the rheological behavior of LDPEs, especially the nonlinear behavior in extensional flow, is highly challenging.

Experimental works for exploring the dynamics of branched polymers in extensional flow have been performed on well-defined model systems [5, 6, 7] as well as commercial polymer systems such as LDPEs. A maximum in the transient extensional stress of LDPE was observed by several groups [8, 9, 10]. Steady stress following the stress overshoot was reported firstly by Rasmussen et al. [11] and has been experimentally confirmed by comparing the measurements from the filament stretching rheometer and the cross-slot extensional rheometer [12], as well as by comparing the constant stretch rate and constant stress (creep) experiments [13]. Several models have been developed [12, 14, 15] for the attempt to understand the physics behind the stress overshoot. However, none of the models can be practically used for predicting the rheological behavior of LDPEs in industry, since the models contain numerous fitting parameters which are not directly related to molecular structures.

Recently Read et al. [16] presented a predictive scheme that is able to calculate the linear and nonlinear viscoelasticity of a stochastically long chain branched polymer melt as a function of the chemical kinetics of its formation. The predictions seem to agree well with the measurements of three LDPEs in both shear and extensional flows. However, the measured extensional data were limited by a maximum Hencky strain of about 3.5, and show no sign of steady state, while the simulations went to much larger Hencky strain values and predicted a steady stress for each strain rate. The quality of predicting the nonlinear behavior at larger Hencky strain values is still unknown. Moreover, in the simulations of Read et al., no stress overshoot was predicted.

In this work, we present extensional measurements for three different commercial LDPEs. The three LDPEs are specially designed based on the predictions of the model in Read et al. [16]. They are expected to have different zero-shear-rate viscosity, but similar stress-strain response in large deformations in nonlinear extensional flow. The measurements are performed on three different devices including two filament stretching rheometers and an extensional viscosity fixture. We show that the measurements from the filament stretching rheometers can reach large Hencky strain values above 5, where the nonlinear steady state is reached. We also show that the LDPE samples have similar nonlinear behavior at large Hencky strain values in extensional flow, including the same magnitude of stress overshoot and the same steady stress following the overshoot, although the Read model predicts no stress overshoot. The results suggest that the nonlinear viscoelasticity of LDPE melts can be controlled through selective polymerization schemes.

2 Experimental

2.1. Materials

Three types of commercial LDPE resins, labeled as PE-A, PE-B and PE-C, have been provided by Dow. All samples were supplied in pellets. Table 1 summarizes the properties of the samples, including the density, the melt flow index (I_2), the weight-average molecular weight (M_w), the number-average molecular weight (M_n), and the melt strength. The weight-average molecular weight is determined by multi angle laser light scattering, while the number-average molecular weight is determined by differential refractive index. The molar mass values are average numbers of several repeats. The melt strength is measured with the Goettfert Rheotens in combination with the Gottfert ALR-MBR 71.92 extruder. Measurements are performed at 150 °C with an output of 600gr/hr. The die has a length of 30 mm and a diameter of 2.5 mm. The experiments have been done with an acceleration of 24mm/s^2. The spin line length is set to 100 mm. The Rheotens tests are performed after an initial purging of the MBR extruder system for 30 minutes and run until failure of the strand. A 4-parameter cross function is fitted through the force-draw down velocity data and the force at failure is determined from the fitted curve at the velocity of failure. The data in the table are average numbers of 5 consecutive measurements.

Table 1: The properties of the LDPE samples

Sample	Density [g/cc]	I_2[dg/min]	M_w[kg/mol]	M_w/M_n	Melt strength [cN]
PE-A	0.920	2.0	160	11	34
PE-B	0.919	8.5	310	22	19
PE-C	0.918	3.9	180	15	26

2.2. Mechanical spectroscopy

The linear viscoelastic (LVE) properties of the three LDPE samples were obtained from small amplitude oscillatory shear (SAOS) measurements. A 25mm plate-plate geometry was used on an ARES-G2 rheometer from TA instruments. The measurements were performed at different temperatures between 130 °C and 190 °C under nitrogen. For each sample, the data was shifted to a single master curve at the reference temperature $T_r = 150$ °C using the time-temperature superposition (TTS) procedure. The time-temperature shift factors (a_T) for all the samples were found to be in agreement with a single Arrhenius equation of the form

$$a_T = \exp\left[\frac{\Delta H}{R}\left(\frac{1}{T} - \frac{1}{T_r}\right)\right], \tag{1}$$

where the activation energy $\Delta H = 65$ kJ/mol. R is the gas constant and T is the temperature in Kelvin. The shift factor a_T is plotted as a function of the temperature in Figure 1.

2.3. Extensional stress measurements

The extensional stress measurements were performed using three different devices: an extensional viscosity fixture (EVF) from TA instruments, a home made filament stretching rheometer (DTU-FSR) [17], and a

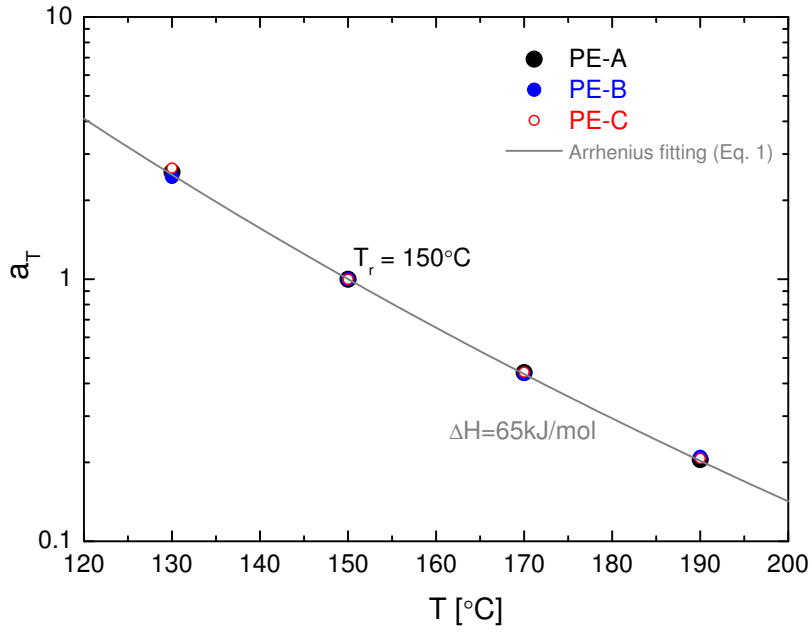

Figure 1: The time-temperature shift factor a_T as a function of the temperature for all the samples. The reference temperature is $T_r = 150\,^{\circ}\mathrm{C}$.

commercial filament stretching rheometer (VADER-1000) from Rheo Filament. Results from the different devices were compared with each other.

The samples for the EVF measurements are compression molded at 150 °C, 3 minutes at low pressure 10bar, 1 minute at high pressure 150bar, then quench cooled to room temperature at 150bar with a quench cool casette. For a short time the samples experience a pressure loss when the cooling casette is inserted. The short time compression molding at relatively low temperature is to prevent any potential oxidation or degradation of the samples. The samples mold is Teflon coated with dimensions of 100 x 100 x 0.5mm. Samples of 12.7 - 12.8mm width are stamped out the plaque of about 20mm long. The final samples thickness is about 0.6mm. In the EVF measurement, a sample is inserted into the device and after a equilibrium time of 180s at 150 °C, the sample is pre-stretched for 15.44s at a strain rate of $0.005s^{-1}$, followed by a relaxation of 80s. Then the sample is stretched. The Hencky strains reported are computed from the cylinder rotations.

Typically extensional measurements using an EVF are limited to the cases where the sample remains homogeneous. The value of the Hencky strain that the EVF can reach in a single revolution is typically below 4. In contrast to the EVF, the filament stretching instruments do not rely on an assumption of homogeneous deformation along the stretching direction. In fact due to the no-slip condition on the plates, the deformation will have to be non-uniform in the axial direction. The devices merely probe the relation between deformation and stress in the plane of minimum diameter typically found in the mid-filament plane. The remaining material outside of this plane is needed just to hold on to the thin slice under investigation in much the same way that a dog-bone shape is used to hold on the material in solid mechanics testing. The filament stretching devices do rely on an assumption of radially homogeneous deformation in the minimum diameter plane. Simulations by Kolte et al. [18]. have shown little if any radial stress variation in the mid-filament plane. A laser micrometer is used to measure the diameter of the thin mid-filament slice. In order to explore higher strains, an online control scheme, which was firstly used by Bach et al. [19] and later published by Marin et al.[20], is employed in both DTU-FSR and VADER-1000 to control the diameter at the mid-plane of the filament during stretching, so that a constant strain rate is ensured before sample breaking. Depending on the types of samples, the maximum value of Hencky strain that both DTU-FSR and VADER-1000 can reach is up to 7.

Prior to making a measurement on the filament stretching rheometers, the samples are hot pressed

into cylindrical test specimens with a radius of R_0 and a length of L_0. The aspect ratio is defined as $\Lambda_0 = L_0/R_0$. The samples are pressed at 150 °C and annealed at the same temperature for 10 minutes and then cooled to room temperature. In the measurements, all the samples are heated up to 150 °C, and after a equilibrium time of 180s, the samples are pre-stretched to a radius of R_p prior to the extensional experiments. For DTU-FSR, $R_0 = 4.5$mm, $L_0 = 2.5$mm and R_p is between 3mm and 4.5mm, while for VADER-1000, $R_0 = 3.0$mm, $L_0 = 1.5$mm and $R_p = 2.5$mm. During the extensional measurements, the force $F(t)$ is measured by a load cell and the diameter $2R(t)$ at the mid-filament plane is measured by a laser micrometer. At small deformation in the startup of the elongational flow, part of the stress difference comes from the radial variation due to the shear components in the deformation field. This effect may be compensated by a correction factor as described in Ref. [21]. For large strains, the correction vanishes and the radial variation of the stress in the symmetry plane becomes negligible [18]. For all the samples in this work, the correction is less than 4% when the Hencky strain value is bigger than 2. The Hencky strain and the mean value of the stress difference over the mid-filament plane are calculated as

$$\epsilon\left(t\right) = -2\ln\left(R\left(t\right)/R_p\right) \tag{2}$$

and

$$\left\langle \sigma_{zz} - \sigma_{rr} \right\rangle = \frac{F\left(t\right) - m_f g/2}{\pi R(t)^2} \cdot \frac{1}{1 + \left(R\left(t\right)/R_0\right)^{10/3} \cdot \exp\left(-\Lambda_0^3\right)/\left(3\Lambda_0^2\right)}, \tag{3}$$

where m_f is the weight of the filament and g is the gravitational acceleration. The strain rate is defined as $\dot{\epsilon} = d\epsilon/dt$. The extensional stress growth coefficient is defined as $\bar{\eta}^+ = \left\langle \sigma_{zz} - \sigma_{rr} \right\rangle/\dot{\epsilon}$.

3 Results and discussion

3.1. Linear viscoelasticity

Figure 2(a) shows the storage modulus G' and loss modulus G" as a function of the angular frequency ω for all the samples at the reference temperature 150 °C. The corresponding complex viscosity η^* is plotted in Figure 2(b). The solid lines in the figures are the results of multimode Maxwell fitting. The multimode Maxwell relaxation modulus $G(t)$ is given by

$$G(t) = \sum_{i=1}^{10} g_i e^{-t/\tau_i}, \tag{4}$$

where g_i and τ_i are listed in Table 2. The zero-shear-rate viscosity η_0 in the table is calculated by

$$\eta_0 = \sum_{i=1}^{10} g_i \tau_i. \tag{5}$$

In Figure 2(b), it is clear that the three samples have different zero-shear-rate viscosity. However, in both Figures 2(a) and 2(b), it seems that the linear behavior of PE-C approaches PE-A at lower frequencies and overlaps PE-B at higher frequencies. Moreover, at $\omega > 1$ rad/s, both the G' and G" curves of PE-C are almost parallel with PE-A with a vertical shift factor of about 0.6.

3.2. Startup and steady-state extensional flow

Figure 3(a) shows the extensional stress growth coefficient as a function of time for PE-A at 150 °C. The measurements from the EVF, DTU-FSR and VADER-1000 are compared in the figure. The dashed line in the figure is the LVE envelope calculated from the Maxwell relaxation spectrum listed in Table 2. The measurements from the EVF are limited by the maximum Hencky strain of 4, and clear to see in Figure 3(b), where the measured stress is plotted as a function of Hencky strain. The measurements from the two filament stretching rheometers are able to reach larger Hencky strain values above 5, where the steady stress is observed.

We note a significant deviation between the EVF and filament stretching measurements. We believe the stress measured by the EVF is too low, especially at low strain rates, which was also observed by Hoyle

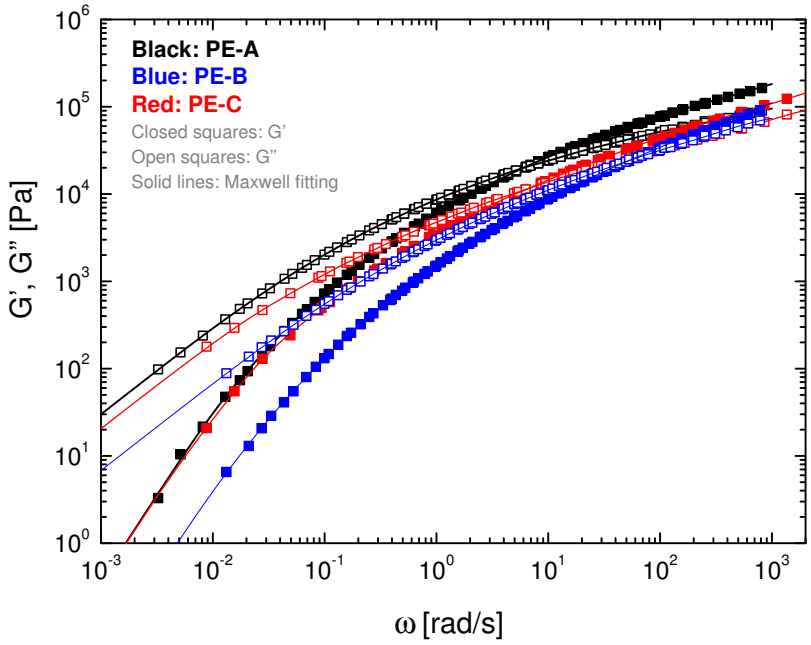

(a)

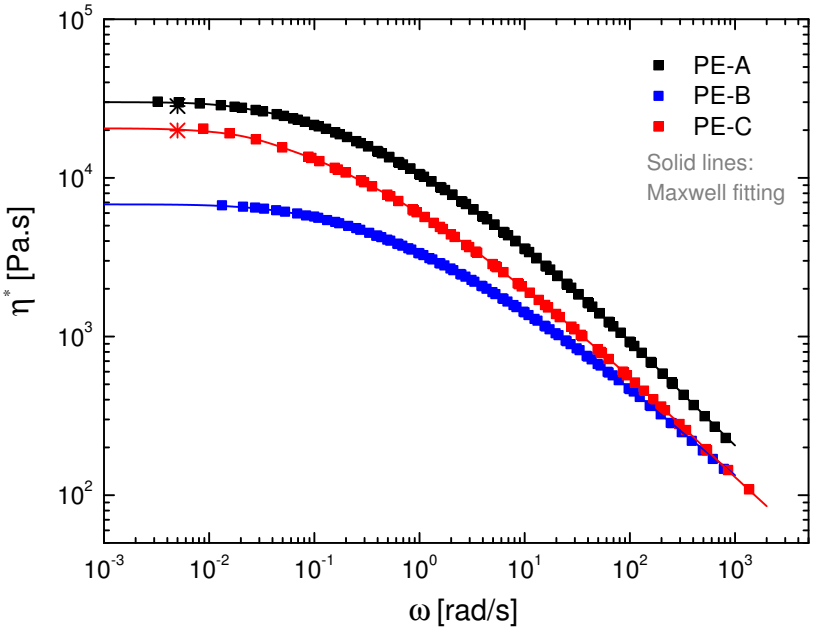

(b)

Figure 2: (a) Storage modulus G' and loss modulus G" as a function of angular frequency ω for all the samples at 150 °C; (b) Complex viscosity η^* as a function of angular frequency ω for all the samples at 150 °C. The two star symbols in the figure are from steady shear measurements with shear rate 0.005 s^{-1} at 150 °C.

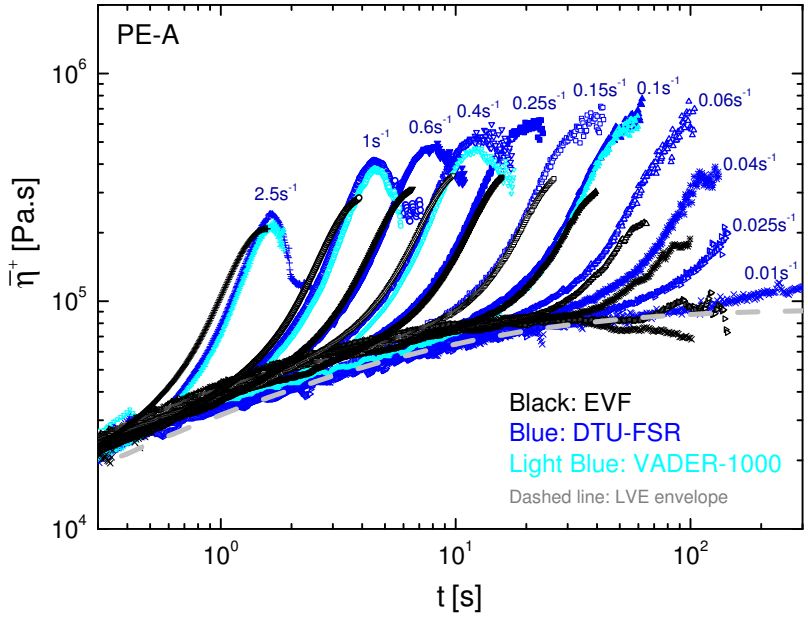

(a)

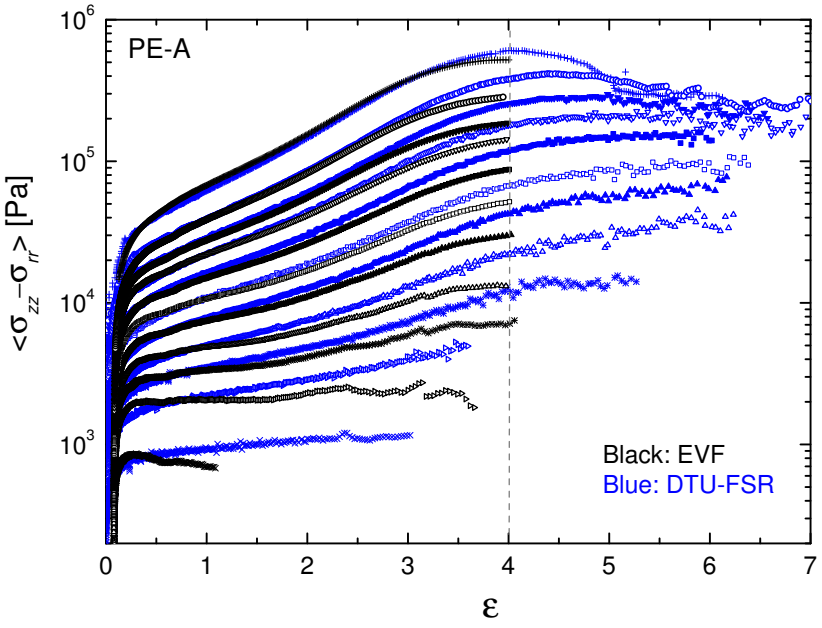

(b)

Figure 3: (a) The measured extensional stress growth coefficient as a function of time for PE-A at 150 °C; Strain rate (from left to right) for both EVF and DTU-FSR: 2.5, 1.0, 0.6, 0.4, 0.25, 0.15, 0.1, 0.06, 0.04, 0.025, 0.01 s^{-1}; for VADER-1000: 2.5, 1.0, 0.4, 0.1 s^{-1};(b) The measured stress as a function of Hencky strain. Strain rate for both EVF and DTU-FSR (from top to bottom): 2.5, 1.0, 0.6, 0.4, 0.25, 0.15, 0.1, 0.06, 0.04, 0.025, 0.01 s^{-1}

Table 2: Linear viscoelastic spectrum for the LDPE melts at 150 °C

Sample	PE-A		PE-B		PE-C	
	τ_i[s]	g_i[Pa]	τ_i[s]	g_i[Pa]	τ_i[s]	g_i[Pa]
	0.00049	$1.690 \cdot 10^5$	0.00063	$1.291 \cdot 10^5$	0.00015	$2.040 \cdot 10^5$
	0.00208	$5.720 \cdot 10^4$	0.00225	$3.212 \cdot 10^4$	0.00068	$6.017 \cdot 10^4$
	0.00885	$4.801 \cdot 10^4$	0.00810	$2.469 \cdot 10^4$	0.00310	$4.023 \cdot 10^4$
Relaxation	0.03759	$2.824 \cdot 10^4$	0.02913	$1.289 \cdot 10^4$	0.01415	$2.518 \cdot 10^4$
spectrum	0.15969	$1.645 \cdot 10^4$	0.10469	$6.611 \cdot 10^3$	0.06469	$1.333 \cdot 10^4$
	0.67846	$7.491 \cdot 10^3$	0.37625	$2.931 \cdot 10^3$	0.29571	$6.693 \cdot 10^3$
	2.88252	$2.799 \cdot 10^3$	1.35227	$1.092 \cdot 10^3$	1.35170	$2.857 \cdot 10^3$
	12.2467	$6.631 \cdot 10^2$	4.86012	$3.257 \cdot 10^2$	6.17870	$9.183 \cdot 10^2$
	52.0312	$8.456 \cdot 10^1$	17.4675	$5.342 \cdot 10^1$	28.2432	$2.327 \cdot 10^2$
	221.060	$1.503 \cdot 10^{-1}$	62.7790	$4.620 \cdot 10^0$	129.101	$7.952 \cdot 10^0$
η_0[Pa.s]	$3.002 \cdot 10^4$		$6.807 \cdot 10^3$		$2.053 \cdot 10^4$	

et al. [12] where the filament stretching measurements were compared with the Sentmanat elongational rheometer measurements. Thus for $\dot{\epsilon} = 0.01\text{s}^{-1}$ in Figure 3(b) , there is deviation already from $\epsilon = 0.5$, while for $\dot{\epsilon} = 2.5\text{s}^{-1}$, the EVF measurement agrees with the DTU-FSR measurement up to $\epsilon = 3.5$. Keep in mind that in EVF only the initial area of the cross-section is known; the changing of cross-section area during stretching is not measured, but calculated from an equation assuming constant stretch rate in homogeneous uniaxial extension. Moreover, in our EVF measurements, the sample width of 12.8mm slightly exceeds the upper limit of 12.7mm as suggested by Yu et al. [22]. This leads to a planar extension rather than a uniaxial extension at larger Hencky strain values. By contrast, in DTU-FSR and VADER-1000, the mid-diameter is measured all the time, so the actual area of the cross-section during stretching is known, whereby the true Hencky strain in the mid-filament plane is computed. With the aid of the online control scheme, a constant ture Hencky strain rate in uniaxial extension is ensured during the whole measurement. The data from DTU-FSR and VADER-1000 at large Hencky strain values are somewhat scattering due to the low force.

In addition, at stretch rates faster than 0.4s^{-1}, a stress overshoot is observed from the measurements using DTU-FSR and VADER-1000. The measurements using the two filament stretching rheometers were not performed at stretch rates faster than 2.5s^{-1}, due to the limitation of the control scheme employed in the apparatus. In filament stretching, surface tension may contribute to the measured stress especially at large Hencky strain values when the radius of the mid-filament plane is very small. Among all the measurements, the smallest radius is $R = 0.12$mm. If we take surface tension $\gamma = 0.03\text{J/m}^2$ for LDPE, the maximum stress from surface tension effect is $\sigma_{\text{sur}} = \gamma/R = 250$Pa. In Figure 3(b), it is clear that for all the measurements that reached Hencky strain more than 4, the measured stress is above 10^4Pa. Therefore the surface tension effect can be neglected.

Figure 4 shows the extensional stress growth coefficient as a function of time for PE-C at 150 °C. The measurements from DTU-FSR and VADER-1000 agree with each other well. The measurements from the EVF agree with DTU-FSR at intermediate stretch rate between 0.15 and 2.5s^{-1}. At stretch rate lower than 0.1s^{-1}, the deviation becomes larger and larger. Stress overshoots are again observed at stretch rates faster than 0.4s^{-1} from the measurements by DTU-FSR and VADER-1000.

The nonlinear behavior of PE-A and PE-C in extensional flow measured by DTU-FSR are compared in Figure 5. As shown in Figure 2, PE-A and PE-C have different linear viscoelastic properties, which is also indicated by the different LVE envelopes in Figure 5(a). In the startup of extensional flows, PE-A and PE-C also have different nonlinear responses. It is clear in Figure 5(a) that PE-C has more significant strain hardening than PE-A for all the stretch rates presented. However, in both Figure 5(a) and 5(b), it is interesting to see that although PE-A and PE-C initially have different nonlinear behavior, they have identical response at larger Hencky strain values, and reach the same extensional steady-state viscosity for each strain rate as shown in Figure 6. Figure 6 also shows that at fast strain rate, the extensional steady-state viscosity exhibits a power-law behavior with the viscosity scaling approximately as $\dot{\varepsilon}^{-0.6}$, which agrees with the observations reported in Ref. [11, 13]. It should be noted that the identical nonlinear behavior is only observed at Hencky strain values bigger than 4 as shown in Figure 5(b), which cannot be measured by the EVF.

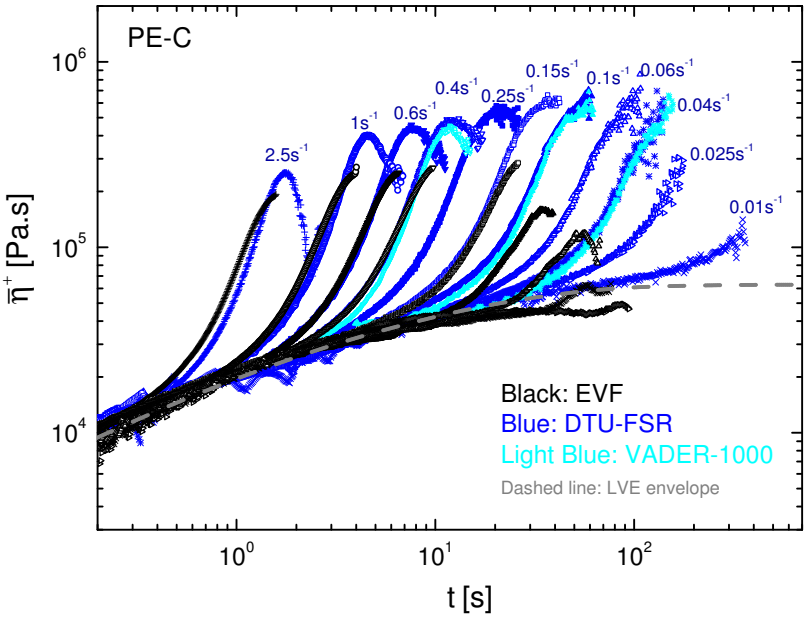

Figure 4: The measured extensional stress growth coefficient as a function of time for PE-C at 150 °C; Strain rate (from left to right) for EVF: 2.5, 1.0, 0.6, 0.4, 0.15, 0.1, 0.06, 0.04, 0.025 s^{-1}; for DTU-FSR: 2.5, 1.0, 0.6, 0.4, 0.25, 0.15, 0.1, 0.06, 0.04, 0.025, 0.01 s^{-1}; for VADER-1000: 0.4, 0.1, 0.04 s^{-1}.

Figure 7(a) compares the extensional stress growth coefficient of PE-B with PE-C at 150 °C. PE-B does not show any stress overshoot for the rates presented. Although PE-B and PE-C behave differently in both linear and nonlinear rheology, it seems that their relative amount of strain hardening is similar at each stretch rate. It is more clearly seen in Figure 7(b), where the Trouton ratio is compared. The Trouton ratio is defined as $Tr = \bar{\eta}^+/\eta_0$, where η_0 is the zero-shear-rate viscosity and the values are listed in Table 2. It can be seen that at each stretch rate, PE-B reaches the same maximum Trouton ratio as PE-C, confirming that they have the same relative amount of strain hardening.

4 Conclusions

We have measured the extensional rheology of three commercial LDPE samples using three different devices. The three devices gave consistent results in the startup of extensional flow. However, the measurements from the EVF are limited by the maximum Hencky strain of 4, while the two filament stretching rheometers reach larger Hencky strain values where the stress overshoot and steady-state viscosity are observed. Moreover the EVF measurements follow the filament stretching measurements only up to a strain that depends on the strain rate. Although the three LDPE samples have different linear viscoelastic properties, it has been shown that PE-A and PE-C have very similar nonlinear rhelogical behavior at Hencky strain values bigger than 4, while PE-B and PE-C have the same relative amount of strain hardening. The results presented suggest that the nonlinear rheology of industrial LDPEs can be tuned by polymerization. In particular it is possible to synthesize a polymer (PE-C) that has substantially lower viscoelastic moduli than a reference polymer (PE-A), but yet has an identical extensional viscosity to the reference.

Acknowledgement

Financial support from the Aage og Johanne Louis-Hansen Foundation is gratefully acknowledged. We thank Dr. Jaap den Doelder from Dow Benelux BV for selecting the resins and the instructive comments.

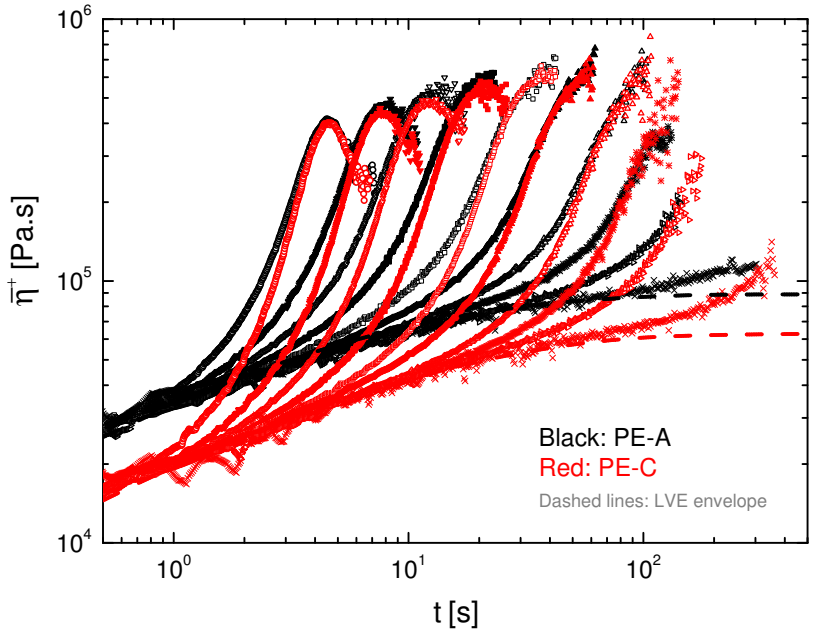

(a)

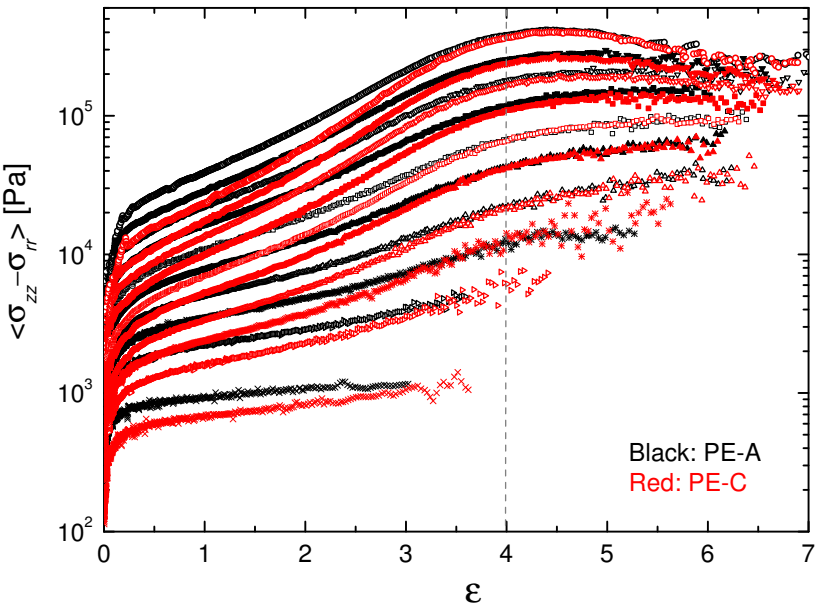

(b)

Figure 5: Comparison of PE-A and PE-C (both measured by DTU-FSR) at 150 °C: (a) The measured extensional stress growth coefficient as a function of time; Strain rate (from left to right): 1.0, 0.6, 0.4, 0.25, 0.15, 0.1, 0.06, 0.04, 0.025, 0.01 s^{-1}; (b) The measured stress as a function of Hencky strain; Strain rate (from top to bottom): 1.0, 0.6, 0.4, 0.25, 0.15, 0.1, 0.06, 0.04, 0.025, 0.01 s^{-1}

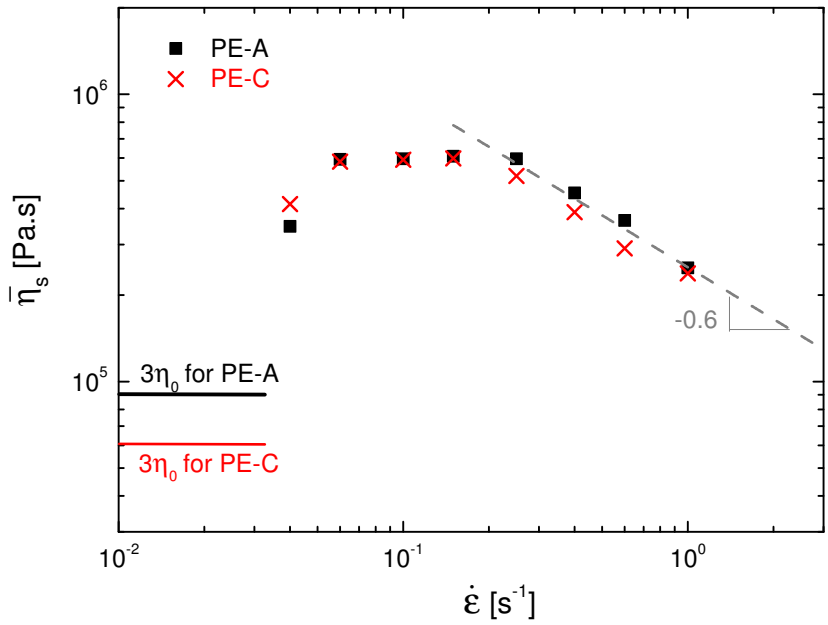

Figure 6: Comparison of the extensional steady-state viscosity as a function of strain rate between PE-A and PE-C at 150 °C.

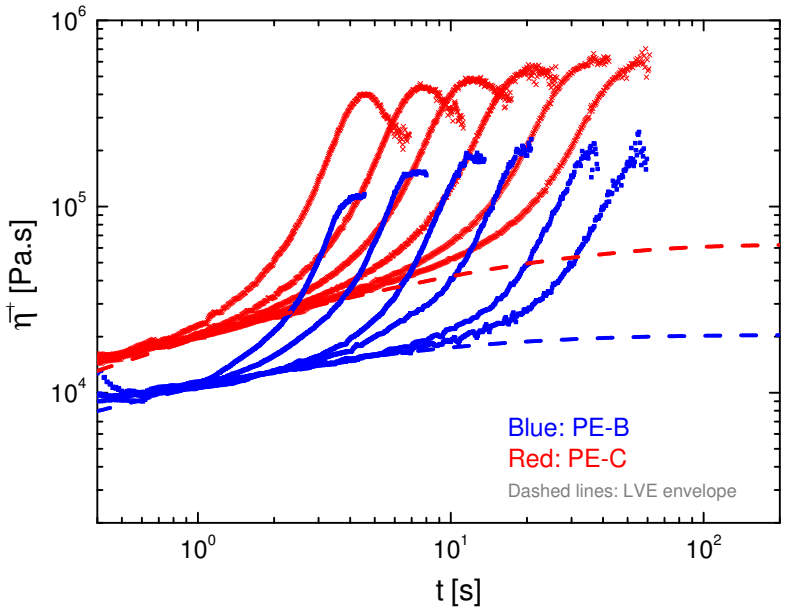

(a)

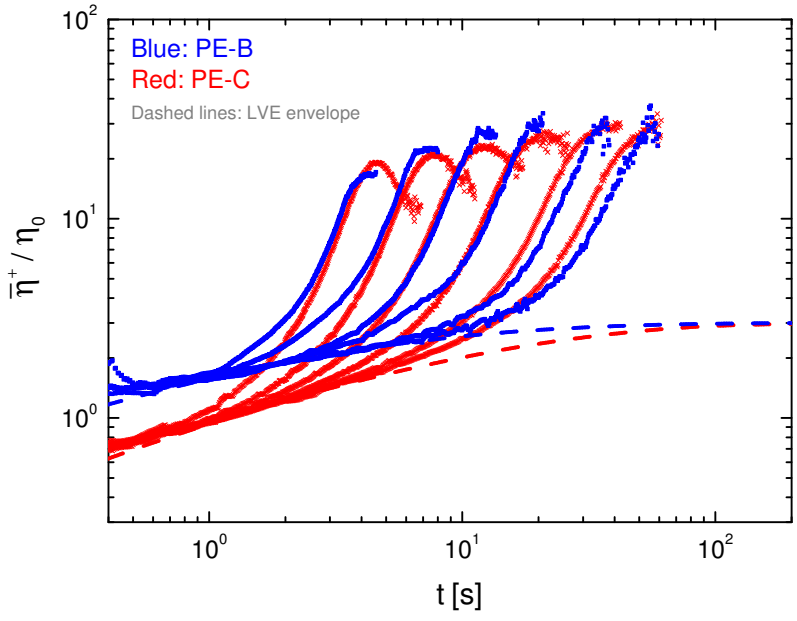

(b)

Figure 7: Comparison of PE-B and PE-C at 150 °C: (a) The measured extensional stress growth coefficient as a function of time; Strain rate (from left to right): 1.0, 0.4, 0.15, 0.1, 0.04 s^{-1}; (b) The measured Trouton ratio as a function of time; Strain rate (from left to right): 1.0, 0.4, 0.15, 0.1, 0.04 s^{-1}.

References

[1] Doi, M.; Edwards, S. F. The Theory of Polymer Dynamics. Clarendon Press: Oxford, U.K., 1986.

[2] de Gennes, P. G. J. Chem. Phys. 1971, 55, 572.

[3] Huang, Q.; Mednova, O; Rasmussen, H. K.; Alvarez, N. J.; Skov, A. L.; Almdal, K.; Hassager, O. Macromolecules 2013, 46, 5026–5035.

[4] Huang, Q.; Alvarez, N. J.; Matsumiya„Y.; Rasmussen, H. K.; Watanabe, H.; Hassager, O. ACS Macro Lett. 2013, 2, 741–744.

[5] Nielsen, J. K.; Rasmussen, H. K.; Denberg, M.; Almdal, K.; Hassager, O. Macromolecules 2006, 39, 8844–8853.

[6] Van Ruymbeke, E.; Muliawan, E. B.; Hatzikiriakos, S. G.; Watanabe, T.; Hirao, A.; Vlassopoulos, D. J. Rheol. 2010, 54, 643–662.

[7] Lentzakis, H.; Vlassopoulos, D.; Read, D. J.; Lee, H.; Chang, T.; Driva, P.; Hadjichristidis, N. J. Rheol. 2013, 57, 605–625.

[8] Raible, T.; Demarmels, A.; Meissner, J. Polym. Bull. 1979, 1, 397–402.

[9] Meissner, J.; Raible, T.; Stephenson, S. E. J. Rheol. 1981, 25, 1–28.

[10] Münstedt, H.; Laun, H. M. Rheol. Acta 1981, 20, 211–221.

[11] Rasmussen, H. K.; Nielsen, J. K.; Bach, A.; Hassager, O. J. Rheol. 2005, 49, 369–381.

[12] Hoyle, D. M.; Huang, Q.; Auhl, D.; Hassell, D.; Rasmussen, H. K.; Skov, A. L.; Harlen, O. G.; Hassager, O.; McLeish, T. C. B. J. Rheol. 2013, 57, 293–313.

[13] Alvarez, N. J.; Román Marín, J. M.; Huang, Q.; Michelsen, M. L.; Hassager, O. Phys. Rev. Lett 2013, 110, 168301.

[14] Wagner, M. H.; Raible, T.; Meissner, J. Rheol. Acta 1979, 18, 427–428.

[15] Hawke, L. G. D.; Huang, Q.; Hassager, O.; Read, D. J. J. Rheol. 2015, 59, 995–1017.

[16] Read, D. J.; Auhl, D.; Das, C.; den Doelder, J.; Kapnistos, M.; Vittorias, I.; McLeish, T. C. B. Science 2011, 333, 1871–1874.

[17] Bach, A.; Rasmussen, H. K.; Hassager, O. J. Rheol. 2003, 47, 429–441.

[18] Kolte, M. I.; Rasmussen, H. K.; Hassager, O. Rheol. Acta 1997, 36, 285–302.

[19] Bach, A.; Almdal, K.; Rasmussen, H. K.; Hassager, O. Macromolecules 2003, 36, 5174–5179.

[20] Román Marín, J. M.; Huusom, J. K.; Alvarez, N. J.; Huang, Q.; Rasmussen, H. K.; Bach, A.; Skov, A. L.; Hassager, O. J. Non-Newtonian Fluid Mech. 2013, 194, 14–22.

[21] Rasmussen, H. K.; Bejenariu, A. G.; Hassager, O.; Auhl, D. J. Rheol. 2010, 54, 1325–1336.

[22] Yu, K.; Román Marín, J. M.; Rasmussen, H. K.; Hassager, O. J. Non-Newtonian Fluid Mech. 2010, 165, 14–23.